NASA/TM—2004-213126 AIAA–2004–3016

Effect of Heating on Turbulent Density Fluctuations and Noise Generation From High Speed Jets

Jayanta Panda
Ohio Aerospace Institute, Brook Park, Ohio

Richard G. Seasholtz
Glenn Research Center, Cleveland, Ohio

Kristie A. Elam
Akima Corporation, Fairview Park, Ohio

Amy F. Mielke
Glenn Research Center, Cleveland, Ohio

Dennis G. Eck
QSS Group, Inc., Cleveland, Ohio

June 2004

The NASA STI Program Office . . . in Profile

Since its founding, NASA has been dedicated to the advancement of aeronautics and space science. The NASA Scientific and Technical Information (STI) Program Office plays a key part in helping NASA maintain this important role.

The NASA STI Program Office is operated by Langley Research Center, the Lead Center for NASA's scientific and technical information. The NASA STI Program Office provides access to the NASA STI Database, the largest collection of aeronautical and space science STI in the world. The Program Office is also NASA's institutional mechanism for disseminating the results of its research and development activities. These results are published by NASA in the NASA STI Report Series, which includes the following report types:

- TECHNICAL PUBLICATION. Reports of completed research or a major significant phase of research that present the results of NASA programs and include extensive data or theoretical analysis. Includes compilations of significant scientific and technical data and information deemed to be of continuing reference value. NASA's counterpart of peer-reviewed formal professional papers but has less stringent limitations on manuscript length and extent of graphic presentations.

- TECHNICAL MEMORANDUM. Scientific and technical findings that are preliminary or of specialized interest, e.g., quick release reports, working papers, and bibliographies that contain minimal annotation. Does not contain extensive analysis.

- CONTRACTOR REPORT. Scientific and technical findings by NASA-sponsored contractors and grantees.

- CONFERENCE PUBLICATION. Collected papers from scientific and technical conferences, symposia, seminars, or other meetings sponsored or cosponsored by NASA.

- SPECIAL PUBLICATION. Scientific, technical, or historical information from NASA programs, projects, and missions, often concerned with subjects having substantial public interest.

- TECHNICAL TRANSLATION. English-language translations of foreign scientific and technical material pertinent to NASA's mission.

Specialized services that complement the STI Program Office's diverse offerings include creating custom thesauri, building customized databases, organizing and publishing research results . . . even providing videos.

For more information about the NASA STI Program Office, see the following:

- Access the NASA STI Program Home Page at ***http://www.sti.nasa.gov***

- E-mail your question via the Internet to help@sti.nasa.gov

- Fax your question to the NASA Access Help Desk at 301–621–0134

- Telephone the NASA Access Help Desk at 301–621–0390

- Write to:
  NASA Access Help Desk
  NASA Center for AeroSpace Information
  7121 Standard Drive
  Hanover, MD 21076

NASA/TM—2004-213126 AIAA–2004–3016

Effect of Heating on Turbulent Density Fluctuations and Noise Generation From High Speed Jets

Jayanta Panda
Ohio Aerospace Institute, Brook Park, Ohio

Richard G. Seasholtz
Glenn Research Center, Cleveland, Ohio

Kristie A. Elam
Akima Corporation, Fairview Park, Ohio

Amy F. Mielke
Glenn Research Center, Cleveland, Ohio

Dennis G. Eck
QSS Group, Inc., Cleveland, Ohio

Prepared for the
Tenth Aeroacoustics Conference
cosponsored by the American Institute of Aeronautics and Astronautics
and the Confederation of European Aerospace Societies
Manchester, United Kingdom, May 10–12, 2004

National Aeronautics and
Space Administration

Glenn Research Center

June 2004

Available from

NASA Center for Aerospace Information
7121 Standard Drive
Hanover, MD 21076

National Technical Information Service
5285 Port Royal Road
Springfield, VA 22100

Available electronically at http://gltrs.grc.nasa.gov

Effect of Heating on Turbulent Density Fluctuations and Noise Generation From High Speed Jets

Jayanta Panda
Ohio Aerospace Institute
Brook Park, Ohio 44142

Richard G. Seasholtz
National Aeronautics and Space Administration
Glenn Research Center
Cleveland, Ohio 44135

Kristie A. Elam
Akima Corporation
Fairview Park, Ohio 44126

Amy F. Mielke
National Aeronautics and Space Administration
Glenn Research Center
Cleveland, Ohio 44135

Dennis G. Eck
QSS Group, Inc.
Brook Park, Ohio 44142

ABSTRACT

Heated jets in a wide range of temperature ratios (TR), and acoustic Mach numbers (M_a) were investigated experimentally using far field microphones and a molecular Rayleigh scattering technique for turbulent density fluctuation measurements. Two sets of operating conditions were considered. For the first set, the temperature ratio, defined as a ratio of plume static temperature to ambient temperature, was varied between $0.84 \leq TR \leq 2.7$ while the acoustic Mach number, defined as a ratio of jet velocity to ambient sound velocity, was kept fixed at $M_a = 0.9$. For the second set M_a was varied between 0.6 and 1.48, while temperature ratio was kept fixed at 2.27. The implementation of the molecular Rayleigh scattering technique required special attention to clean the primary jet as well as the entrained air from dust particles. Additionally, a hydrogen combustor was used to avoid soot particles. The intensity of light scattered by gas molecules in air was measured to determine time-variation of air density fluctuations. Time averaged density measurements in the first set of data showed differences in the peripheral density shear layers between the unheated and heated jets. While radial profiles from all heated jets were nearly similar, those of the unheated jet lie closer to the jet axis. The initial shear layer close to the nozzle exit showed increasing turbulence level with increasing plume temperature. This is opposite to the initial expectation of lowering turbulence level due to the lowering in Reynolds number associated with heating. Further downstream the density fluctuations spectra are found to be nearly identical for all Mach number and temperature ratio conditions. This was in contrast to the significant changes in far field noise radiation found in these jets. At constant $M_a = 0.9$ the high frequency part of the far field noise from jets of different temperature ratio shows significant reduction at all polar angles; the low Strouhal frequency part was nearly identical at shallow radiation angles. To determine noise sources a correlation study between air density fluctuations inside the jet and far field sound pressure fluctuations was conducted. The correlation data, expressed in coherence spectra, was able to determine sources for the low frequency noise (Strouhal frequency < 0.8). For all jets the core region beyond the end of the potential flow was found to be the strongest noise source. Except for an isothermal jet, the coherence spectra from various positions of the plume did not differ significantly with increasing temperature ratio. The isothermal jet created little density fluctuations. Although the far field noise from this jet did not show any exceptional trend, the flow-sound correlations were very low. This indicated that the density fluctuations only acted as a 'tracer parameter' for the noise sources. The correlation data from jets with variable M_a but fixed temperature ratio were similar to the measurements done in unheated jets by Panda and Seasholtz (JFM, 2002).

INTRODUCTION

The noise emitted by the exhaust plume from a gas turbine engine continues to be a significant contributor to the total radiation from current commercial airplanes. This is expected to be a bigger problem for the future commercial supersonic flights with lower bypass ratio engines. On the other hand, federal regulations and community standards are lowering the acceptable noise thresholds. Therefore, there is a continuous need to further understand the noise generation mechanisms and develop noise reduction technologies. Such technologies are expected to have significant economical impacts. Since the noise generated from the engine plumes shows reasonable scaling with diameter, smaller diameter jets provides an economical basis for laboratory jet noise study.

The present work looks into the effect of varying plume temperature on noise emission. The source for the jet noise is the turbulent fluctuations in the plume and like turbulence, there exists multiple, and sometimes contradictory, descriptions of the noise source. Various acoustic measurements of heated round jets (for example Tanna, 1977 JSV; Fisher et al 1973) have shown two intriguing effects of heating on the far field noise radiations. First, as the plume temperature is increased keeping acoustic Mach number M_a fixed, the overall sound pressure level (OASPL) decreases if $M_a < 0.7$ while an increase is observed for $M_a > 0.7$. The acoustic Mach number is defined as a ratio of jet velocity to ambient sound velocity. Second, the acoustic spectra show an increase in low frequency noise with heating, i.e., the spectral peak shifts to lower frequency with increased heating. Although the second observation is not universally correct (as will be shown later) various researchers

have argued that the experimental data provide support to the existence of a sound source different from the unheated counterpart, and explicable through the second source term, of the stress tensor in Lighthill's acoustic analogy (1954):

$$\frac{\partial^2 \rho}{\partial t^2} - a_0^2 \nabla^2 \rho = \frac{\partial^2 T_{ij}}{\partial X_i \, \partial X_j}; \qquad \textbf{(1)}$$

$$T_{ij} = \rho V_i \, V_j + \delta_{ij}(p - a_0^2 \rho)$$

where, ρ is air density, p is pressure, V_i and V_j are velocity vectors and T_{ij} are the elements of the stress tensor. The above expression neglects the viscous contribution. The second term can be decomposed into density and entropy fluctuations; by changing the plume temperature one affects these two variables, hence the significance of the dipole second source. Crighton (1975) surmises earlier analyses of the second term as noise source in heated jets. Tam (2001), an opponent of the acoustic analogy approach, argues that the analogy equation does not differentiate propagation from sound sources. He supports a 2 scale (large-scale and fine-scale) model based on the structural description of turbulence. The energy containing low frequency part is expected to produce the shallow angle 'large-scale' part of the noise while the smaller eddies produce omni-directive fine-scale noise. The effect of heating is not separately identifiable as in Lighthill's equation. Recently, Viswanathan (2001) focused on the issue of contamination of the earlier acoustic data from various facility-induced sources, and suggested that the extra noise level attributed as dipole source may be due to lower Reynolds number operation associated with small model diameter and lower viscosity at higher temperature. This brings further confusion to the effect of heating on jet noise.

The confusion creates significant impact on the noise prediction tools based on the semi-analytical models and purely computational approaches. Except for the direct numerical simulation, which can only be done for very small Reynolds number situations, all other models depend on different levels of turbulence modeling, length and time scale estimates that can be verified only by comparing with experimental data. So far the bulk of the experimental data are solely in the form of far field noise spectra. To verify any of the noise generation mechanisms, or the assumptions on turbulence modeling, one needs to measure complex turbulent statistics. Yet an aerodynamic measurement tool that can provide simple unsteady statistics is difficult to find. Experimental study of jet noise is therefore tied to instrumentation development. The commercially available Laser Doppler Velocimetry (Kerhervé et al., 2003) and Particle Image Velocimetry (Lourenco and Krothapalli 1995, Bridges and Wernet 2003) have produced time averaged velocity and turbulent kinetic energy measurements; complex statistics have been attempted yet measurement uncertainties are expected to be significant. The present molecular Rayleigh scattering based technique does not require any seed particles, instead light scattered by gas molecules are analyzed to simultaneously measure velocity, temperature and density. The setting up of such a system requires special attention to cleaning the air streams, vibration isolation and other issues. In the past density fluctuations in premixed flames was measured by Rayleigh scattering (Pitts and Kashiwagi, 1984). The present system is far more extensive and elaborate. We have used Rayleigh scattering system extensively to measure time average fields and turbulent statistics in unheated jets (Panda and Seasholtz 2002, henceforward mentioned as PS 2002; Panda, Seasholtz and Elam 2003). By simultaneously acquiring flow turbulence and far field acoustics data, and cross-correlating the two, it was possible to determine the low frequency ($0 < St < 1$) noise sources in unheated jets. Some of the insightful measurements of noise source distribution came from these correlation data. However, all of these efforts were in unheated jets; the present work attempted to do similar measurements in heated jets. The goals of the present work are: (1) to set up a similar Rayleigh scattering system around a bigger and heated jet facility; (2) to create a data base that can be utilized to validate various CFD and CAA codes; (3) to provide physical insights into the effect of heating on jet noise generation.

EXPERIMENTAL SETUP

The experiment was performed in the Small Hot Jet Acoustic Rig in the Aeroacoustics Propulsion Laboratory (AAPL) of NASA Glenn Research Center. AAPL is a 65 ft (20m) radius, anechoic, geodesic-dome. The walls of the dome and approximately half of the floor area are treated with acoustic wedges made from fiberglass wool to render the facility anechoic above 220 Hz. A 60 in. (1.5 m) exhaust fan in the top of the dome provides air circulation. Flows from all rigs are directed out the 55 ft (16.8m) wide by 35 ft (10.7 m) high doorway to an open field (Castner 1994). The jet facility is capable of producing heated jets with total temperature from ambient to 920 K (1650 R) in the Mach number range $0< M < 2$, and therefore ideal for studying the effect of heating. A 2 in. (50.8 mm) diameter convergent nozzle was used for all measurement conditions. The operating conditions are shown in Table I and graphically presented in Figure 1. The choice of the operating conditions is guided by the work of Tanna (1977) and Tanna, Dean and Burrin (1976) who created a far field noise data base from a similar 2 in. diameter nozzle. Bridges and Wernet (2003) have reported time average velocity and turbulent kinetic energy data from PIV tests on many of the operating conditions used in the present test. The test conditions were chosen such that one set reflects the effect of static temperature variation for a constant $M_a = 0.9$, and the second set reflects the effect of jet velocity for constant temperature ratio TR = 2.27. Note that the "Tanna Plot" of figure 1 uses acoustic Mach number M_a, as opposed to jet Mach number M_j (= U_j/a_j, where a_j is the sound speed in the jet core), and jet static temperature ratio TR (= core static temperature T_j/ ambient temperature T_a). Heating not only introduces temperature ratio as a parameter, but a couple of other variables as well. While M_a is the commonly used parameter for sound radiation (that involves coupling between jet velocity and ambient sound speed), the compressibility effect is represented by the jet Mach number M_j. To fix acoustic Mach number, the jet Mach number has to be lowered for higher temperature plumes (Figure 2a). The other effect is a significant reduction of Reynolds number with heating shown in Figure 2(b). The lowering of the Reynolds number has been suspected to relaminarize the initial lip shear layer; therefore, is a source of additional noise.

The far field sound pressure fluctuations were measured by an array of seven ¼ in. (6.35mm) microphones kept on

an arc of 100 D (5.08 m) and centered at the nozzle exit. The microphones were angularly placed with 10° increments: from 150° to 90° to the jet exit* (Figure 3). The presence of the large traversing unit, optical components and other metal surfaces was a concern for significant acoustic reflection. To minimize such reflection a large part of such surfaces were covered by 50mm thick polyurethane foams.

Rayleigh setup: Although Rayleigh scattering can be used to simultaneously measure temperature, density and one component of velocity, it was decided to resort to a setup for density only in this first attempt on a heated jet facility. Once density measurement becomes feasible, by mitigating various issues with particle removal and vibration isolation, velocity and temperature measurements are possible via optical spectral analysis of the collected scattered light.

The principle for air density measurement using Rayleigh scattering is straightforward. The molecules of a gas, under the influence of the electric field of an incident laser beam, become electrical dipoles and radiate at the same frequency as that of the incident field. The total scattered light arriving at a detector is due to the net scattering from the large number of molecules present at the probe volume. The scattered power is proportional to the molecular number density η. The scattered light also has a small inelastic component (at frequencies different from the incident beam), such as due to the Raman scattering. The scattered power from that part, once again, is linearly dependent on η. For a dilute gas, the Rayleigh scattered light P_s, collected from a probe volume, V_{sc} into a solid angle, $d\Omega$, can be written as

$$P_S = \eta\, I_0\, V_{sc}\, \frac{d\sigma}{d\Omega} \sin^2\chi d\Omega = k''' \eta \ . \qquad \textbf{(2)}$$

Here I_0 is the incident light intensity, $d\sigma/d\Omega$ is the differential Rayleigh scattering cross-section of the gas (or gas mixture) under consideration, χ is the angle between the incident electric vector and the direction of light collection, and k''' is a constant. The Rayleigh scattering cross-section depends on the light wavelength and the effective molecular diameter, and is constant for a fixed wavelength laser and a fixed gas mixture (air for this work). The Rayleigh scattering cross-section is very small for gases like N_2 and O_2, and therefore the problem with particles and condensates. For 532 nm incident light, the differential Rayleigh cross section for air is 6.13×10^{-32} m^2/Sr, while that of a micron size particle is many orders of magnitude higher. It is estimated that a 100 nm water droplet present in 0.3 mm × 0.3 mm × 0.3 mm probe volume will dominate scattering from air at atmospheric condition (Miles et al 2001). Therefore precautions had to be taken to avoid particles and water condensation. For the present setup the condensation was absent whenever the combustor was used. Although unheated jets in Mach number $M_a \geq 0.9$ showed trace of fogging.

Soot generation from the combustors was another concern. To avoid soot a hydrogen combustor was used. Burning hydrogen produced steam, which did not condense in the high temperature plume. Note that the Rayleigh scattering cross-section of steam is 13% lower than that of oxygen. Since the combustion process replaced some oxygen by steam, the Rayleigh scattering cross-section for the heated air is expected to be different from the ambient. The difference, however, is calculated to be small (~ 0.5%) even for the maximum jet temperature. No special steps were taken to account for this difference which has manifested as a source of measurement uncertainty.

Neglecting the change in Rayleigh scattering cross-section, equation 2 shows that for a fixed optical setup (fixed incident power, f/# of the collection lens, and beam diameter), the collected light intensity is directly proportional to the molecular number density. The number density η is directly related to bulk density ρ. Photomultiplier tubes and photon counting electronics were used for measuring the scattered power. The number of photo-electrons N arriving over a time interval Δt is directly proportional to the scattered light intensity and therefore, to the bulk density ρ:

$$N = k''\rho\,\Delta t \qquad k'' : \text{constant} \qquad \textbf{(3)}$$

In reality, the Rayleigh scattered light is contaminated by small amount of background light. Therefore the linear relation has two constants k and k' to be determined via calibration in known density flows:

$$N = (k\rho + k')\,\Delta t \qquad \textbf{(4)}$$

The Rayleigh setup was built in two parts: the first is around the jet facility (Figures 4 and 6) and the second part inside a control room away from the facility (Figure 5). A side view of the setup inside the AAPL dome is shown in Figure 3. Dry, compressed air was supplied to the facility from a central air handler. The compressed air was passed through additional 0.3 micron filters for dust removal. Just before the test, the facility was used for PIV study. The interior of a significant part of the facility, from settling chamber to the nozzle lip, was covered by a thick layer of aluminum oxide powder. All components were dismantled, cleaned and reassembled before the test. The seed particles create a general nuisance as every surface of the dome and all wedges are covered by the particles. The cleaning part was only confined to the interior flow passage of the primary jet and nowhere else. Instead the jet was surrounded by a clean co-flow stream from an 11in.×11 in. square opening (Figure 5). The co-flow was created by a separate air blower that took in the ambient air and passed it through a 0.3micron filter. The filtered air was passed to a settling chamber built around the outside of the facility and finally exhausted through the square opening at around 20m/s speed.

Similar to the earlier efforts on unheated jets (PS 2002), the present setup was for a point measurement technique. A continuous wave laser beam was passed normal to the jet axis and the light scattered from a small region on the beam was collected and focused onto an optical fiber. The part of the setup, around the jet facility, was built on a large 2-axis (axial x and radial r) traversing unit that allowed plume survey in one x-r plane. The light source was a solid state, frequency doubled Nd:VO_4 laser that produced 5Watt power at 532 nm wave-

* In our prior publications (PS 2002; Panda, Seasholtz and Elam, 2003) microphone polar angles were measured from the jet flow direction, while for the present document polar angles are presented from the flight direction. While the former is better suited for spherical coordinate specification of noise radiation, the latter is more commonly used in the aircraft community. Nonetheless, 150° in the present paper is equivalent to 30° in the earlier.

length. The laser head was also mounted on the traverse. To avoid damage from the high noise level produced by the jets the laser head was enclosed in an anechoic box (Figures 4 and 6). The incident laser beam was focused at the probe volume by a 500 mm focal length achromat and the polarization was adjusted for maximum scattering intensity towards the 90°, vertically down collection direction. The beam, after crossing the plume, was dissipated in a long and narrow dump (Figure 4). The collection lens consisted of a pair of f/3, 150 mm diameter achromats that focused the collected light on a 550 micron multimode optical fiber. The combination of the fiber diameter and 1:1 imaging fixed the measurement probe volume length to 550 microns. The beam waist was about 150 microns in diameter. Since stray scattering of the incident beam can overwhelm Rayleigh signal, various baffles were created on the transmission path. Except for the portion of the beam that crossed the jet, the rest of the laser path was covered with metal tubes. To avoid collection of stray background light the collection lenses were placed in an enclosure with one end open towards the beam, and a large 380 mm diameter hollow tube, suspended from the top, provided dark background (Figure 6). Additionally to avoid sunlight the entire test was conducted after dark: between 10:30 p.m. and 6 a.m.

The 76 meter long optical fiber passed the collected scattered light to a control room for light intensity measurement (Figure 5). Here the collected light was collimated and then split into two equal parts by a beam splitter. Each of the beams was refocused into individual photomultiplier tubes (PMT). The purpose of two photomultipliers is to reduce the effect of electronic shot noise in density spectrum calculations (PS 2002). Photon counting electronics were used to measure light intensities. Each PMT channel was terminated in a preamplifier and a snubbing circuit to reduce ripples in photoelectron pulses. The preamplifier also provided a small (5×) gain. The pre-amp outputs were passed to constant-fraction discriminators, and finally to a multi-channel, timer-counter board. The counting was performed over a series of contiguous time bins of 10 to 20 microseconds time interval. Usually 1million contiguous bins were used to obtain long time-series data. Before processing, the counts in every bin were corrected for the pulse pile-up error. The entire data collection process was automated to move the laser probe volume from point to point in the flow field, perform the photon-counting process and collect the time histories.

The microphone time signals were acquired by a separate processing and data acquisition system. For correlating the density fluctuations to the far field noise signal, the photoelectron counting and the digitization of the microphone signals had to be synchronized. This was performed in a two step process. First, the timer-counter board for the photo-electron counting was operated from the clock pulses produced by the digitization unit. Second, a single pulse from a separate digital I/O generator initiated both counting and digitization processes. To verify time synchronization a synthetic signal was measured and compared. The synthetic signal was digitized by the microphone signal processor and also used to drive a light emitting diode (LED). The LED produced light intensity modulation at the synthetic signal frequency and was placed in front of a PMT. Finally, the above data acquisition electronics were used to collect microphone and LED signals. Satisfactory synchronization, observed over all frequency ranges tested, provided confidence in the acquisition process.

Signal processing: *Density calibration:* Figure 7 presents typical calibration curves obtained from the two PMT. The laser probe volume was kept at the centerline and about 2 nozzle diameters away from the exit, where the plume density was known from the measured plenum and ambient conditions. For the calibration points (as well as the test points) the jet Mach number was always subsonic Mj < 1; therefore plume properties could be calculated using isentropic relations. Note that such calculations had to account for the lowering of specific heat ratio with increasing temperature. The known plume density was plotted against the average photon arrival rates over 10 second intervals. Least-square linear fits (shown by solid lines) provided calibration constants k_1, k'_1 and k_2, k'_2 for each PMT. Small value of the intercepts k'_1 and k'_2 indicated adequate background suppression. The linearity over a wide density range also indicates satisfactory particle removal from the plume. Usually calibration curves were obtained at the beginning and at the end of each night and were used to convert photo-counts to air density. However, a slight drift in electronics required some checking and adjustment of calibration constants for some sets of data points. The linear dependence of photo-electron count on density made such corrections straightforward. Two different data points: one in the plume core and the other in the ambient co-flow, were sufficient to obtain a new set of calibration constants. This procedure also had to be followed for measurement stations very close to the nozzle exit r/D≤1.0, where a part of the collection lens aperture was blocked by the jet facility resulting in a lower count.

Time averaged measurements: The time averaged density calculation is straightforward from the photo-electron counts (N_i, i = 0, 1, 2, ..n-1; n=1,000,000) performed over contiguous time bins of Δt width. The mean density is related to the average of all bins N_{av} via the calibration constants:

$$\bar{\rho} = \frac{1}{k}\left(\frac{N_{av}}{\Delta t} - k'\right), \quad \text{where, } N_{av} = \frac{\Sigma N_i}{n}. \qquad \textbf{(5)}$$

Since, two PMTs were used for the present setup $\bar{\rho}$ was calculated two times, and an average was finally used. The fundamental source of uncertainty in time-averaged density data is from the electronic shot noise contribution to photo-electron counts. Even when the scattered light is of constant intensity (no density fluctuation) the photo-electron emission rate measured by a PMT shows significant variation. This is referred to as statistical photon count noise or 'shot-noise'. This noise is random in nature and follows Poisson's statistics. An important result of Poisson's statistics is that the variance of shot noise is equal to the time average of all counts:

$$\sigma_{sh}^2 = N_{av} \qquad \textbf{(6)}$$

Hence the relative uncertainty in the measurement of N is

$$\frac{\sigma_{sh}}{N_{av}} = \frac{1}{\sqrt{N_{av}}}. \qquad \textbf{(7)}$$

For the present experiment the count rate was high: between 3 to 12 millions per second. Due to the small time width, the count accumulated in the individual bins was small, yet averaging over

the large number of bins reduced the uncertainty to <0.1%. There was a host of secondary sources that contributed more. The small uncertainty associated with the change in Rayleigh scattering cross-section from the replacement of oxygen by steam has been mentioned earlier. The largest source of uncertainty, however, was from the residual dust particles. In unheated jets, the largest source was a trace of condensation. The passage of a particle through the probe volume manifested as a large spike in photo-electron counts. Such large spikes were removed from the time-series data by neglecting bins with photo-electron counts greater than four times the standard deviation of the series. This rejection process does not account for smaller particles or condensations that may lie just outside of the probe volume and are capable of contaminating the Rayleigh signal. There were also very fine oil droplets, perhaps picked up from the air compressor, caused additional contamination. Although these secondary noise sources are difficult to quantify, the absolute density numbers are found to be repeatable within 2% of their quoted values.

Density fluctuations spectra and rms level measurements: To measure the density fluctuation spectrum and the standard deviation some means of canceling the effect of electronic shot noise is necessary. Towards this goal, another important property is used: shot noises produced by two PMTs are uncorrelated. Therefore when the same light is measured by two PMT, and the two sets of photo-electron counts are cross-correlated, the shot-noise contribution cancels out. The present signal processing scheme used a frequency domain approach, where discrete Fourier transforms $F_{N_1'}$, $F_{N_2'}$ of each set of photo-electron count were performed (the average value needs to be subtracted from the individual count, $N_i' = N_i - N_{av}$)

$$F_{N'}(\ell) = \sum_{i=0}^{m-1} N_i' \exp\left(j\frac{2\pi i \ell}{m}\right), \qquad f_\ell = \frac{1}{m\Delta t} \quad \ell = 0, 1, 2, \ldots \frac{m}{2}-1 \tag{8}$$

The cross spectral density was calculated as

$$\left|P_{N_1'N_2'}(f_\ell)\right| = \frac{2}{m^2}\left|F_{N_1'}(\ell) \cdot F^*_{N_2'}(\ell)\right| \tag{9}$$

Superscript * in the above equation indicates complex conjugate. The power spectrum of air density fluctuation was calculated using appropriate calibration constants k_1 and k_2 for the two photomultiplier tubes

$$P_{\rho^2}(f_\ell) = \frac{\left|P_{N_1'N_2'}(f_\ell)\right|}{k_1 k_2 (\Delta t)^2} \tag{10}$$

Since the mean-square of density fluctuation σ^2_ρ is equal to the total energy in the power spectrum, the root-mean-square of air density fluctuations ρ_{rms} is calculated as follows

$$\sigma_\rho^2 = \sum_{\ell=0}^{\frac{m}{2}-1} P_{\rho^2}(f_\ell), \quad \rho_{rms} = \sqrt{\sigma_\rho^2} \tag{11}$$

The Welch method of modified Periodograms (Welch, 1967) was used to calculate the cross-spectral density. Each long record of photo-electron counts was divided into small segments of m = 512 data points. The adjacent segments were overlapped by 50%. The modified Periodograms of corresponding segments from the two PMTs were calculated and then used to determine local estimates of cross-spectral density. All local estimates were averaged to obtain the final cross-spectral density. A discussion of aliasing error in the spectral calculation can be found in PS 2002.

The rms fluctuation measurement is susceptible to unsteadiness in the laser intensity, which is very small. The major source of error was due to the passage of occasional particles or traces of condensation droplets through the probe volume. The passage of such particles increases the correlated part of the signal in both PMT counts. This leads to a bias towards higher value in the spectrum calculation as well as the root-mean-square calculations. As the probe volume was moved from close to the nozzle exit to 15 diameters downstream, the number of particles increased progressively from a few per second to the order of 1000 per second. As mentioned earlier, signatures of large particles are identifiable in the time series of photo-electron counts and discarded. However, the signature of smaller particles passing through the vicinity of the beam waist could not be discarded. The bias error increased progressively from an insignificant value close to the nozzle exit to >20% farther downstream as a larger number of particles were entrained into the jet. No data were taken beyond a downstream distance of 15D.

Flow-sound correlation measurements: To cross-correlate turbulent density fluctuations ρ' to the far field sound pressure fluctuations p' the spectral approach was once again used. The time series of photo-electron counts and sound pressure data were Fourier transformed: $F_{N_1'}$, $F_{N_2'}$, $F_{p'}$, and the cross-spectrum calculations were performed. Since the collected light was measured with two PMTs, the cross-correlation was performed two times: between microphone signal and either series of counts.

$$P_{N_1'p'}(f_\ell) = \frac{2}{m^2}\left(F_{N_1'}(f_\ell) \cdot F^*_{p'}(f_\ell)\right), \tag{12}$$

where m is the length of data segment used. The coherence spectrum was calculated from the magnitude of the cross-spectrum:

$$\Gamma^2_{\rho'p'}(f_\ell) = \frac{\left|P_{N_1'p'}(f_\ell)\right|^2}{P_{N_1'N_1'}(f_\ell)\; P_{p'p'}(f_\ell)} \tag{13}$$

The Fourier transform and coherence spectrum calculations used the segmenting and averaging process outlined earlier. Finally, an average of the coherence spectrum from the two PMT channels was calculated. Note that the cross-spectrum is unaffected by electronic shot noise which is independent of the noise generation process. (No confusion should be made between 'jet noise' and 'shot noise'; the former is an acoustic phenomenon while the later is photo-electronic in nature). However, to obtain the coherence spectrum the cross-spectrum has to be normalized by the power-spectrum of photo-electron counts (Equation 13). The latter is a sum of power spectra of the air density fluctuations and the spurious electronic shot noise. Therefore, the coherence spectrum becomes biased to a lower value. The biasing error varies between negligible to a large percentage depending on the ratio of air density fluctuations to shot noise floor.

RESULTS AND DISCUSSION:

The following discussion is divided into two parts. The larger first part presents data from jets with different temperature ratios but fixed acoustic Mach number M_a=0.9. Since sound speed in the ambient was nearly constant, fixed M_a implies constant efflux velocity. The second smaller part deals with subsonic jets of different acoustic Mach number but at constant temperature ratio TR = 2.27.

M_a = 0.9 far field acoustics: The effect of heating on the far field noise spectra of a fixed velocity (M_a = 0.9) is shown in Figure 8. The narrowband spectra were obtained from power spectra calculations of the microphone time signals. The frequency values were converted to Strouhal number, St = fD/U_j (f: frequency), and the power spectra $S_{p'^2}$ were converted into spectral density per unit Strouhal frequency $S_{p'^2}/(\Delta f\, D/U_j)$, where Δf is the width of each frequency bin. Interestingly, Figure 8(a) shows that in the shallow angle the low frequency part $0 \le St \le 0.5$ remains nearly unchanged with increasing plume temperature, while the higher frequency part continually decreases. For the 100° location, heating causes progressive lowering of sound emission at all frequencies. The increase in the jet temperature is expected to reduce high frequency radiation from the shallow angles due to increased refraction. However, refraction can not be attributed to the reduction measured by the 100° microphone. The effect of heating at M_a = 0.9 is weakening of the noise sources. A different conclusion can be reached when the effect of the density reduction with increased plume temperature is accounted for. The lowering of air density proportionately reduces the thrust generated by the jet. The thrust (proportional to $\rho_j U_j^2$) produced by the highest temperature plume is expected to be only 31% of that of the unheated counterpart. Additionally the first term of Lighthill's stress tensor is related to $\rho_j U_j^2$; to determine the influence of the second term (the dipole source term) one needs to keep $\rho_j U_j^2$ constant. The data in Figures 8(a) and (b) were obtained with fixed velocity. To account for the density variation noise spectra are normalized following the procedure of Mollo-Christensen and Narasimha (1960) and Zaman and Yu (1985). In this method, the narrow band spectra is normalized by $\rho_j U_j^2$, jet diameter, microphone distance from the nozzle exit R and Strouhal frequency: $\frac{S_{p'^2}}{\left(\rho_j U_j^2\right)^2}\frac{R^2}{D^2}\frac{U_j}{\Delta f\, D}$. Note that the non-dimensionalization does not account for the velocity scaling. Nevertheless, an interesting trend emerges in the shallow angle spectra (Figure 8c). The high frequency parts collapse while the low frequency parts show increasing amplitude with increasing temperature. For the 100° spectra the effect of heating at constant velocity and constant thrust is clearly a broad increase at all frequencies.

The current data were affected by reflections from optics and other hard surfaces as described earlier. Therefore, the far field spectra measured by Tanna were analyzed and the same trends, as described above for the M_a = 0.9 condition, were observed. Clearly, for the shallow 150° angle the low frequency part of the spectra scales with jet velocity and the high frequency part with thrust. The effect of heating on the far field noise is different for different Mach number jets. Far field noise spectra measured by Tanna et al (1976) at 3 Mach numbers and temperature ratios comparable to the present test are shown in the Appendix A.

M_a = 0.9 plume survey: *Time-averaged and rms data:* Figures 9 and 10 present density survey of unheated (TR = 0.84) and heated (TR = 2.7) jets. The unheated jet has a higher core density than the ambient ($\rho_j > \rho_a$) due to isentropic cooling from plenum temperature. The heated jet, on the other hand has a lower density than the ambient ($\rho_j < \rho_a$). The experimental data are non-dimensionalized by the difference between the jet centerline and the ambient density, (ρ_j-ρ_a). The time-averaged data were non-dimensionalized as ($\bar{\rho}$-ρ_a)/(ρ_j-ρ_a). The parameter is unity at the core and drops to zero as the ambient condition is reached, regardless of whether the core density is higher or lower than the ambient. For a similar reason the fluctuating density data were normalized by the absolute value of the density difference: $\rho_{rms}/|(\rho_j-\rho_a)|$. The radial profiles show progressive growth of the lip shear layer and the expected spreading of the plumes. Because of the condensation problem, the unheated jet data of Figure 9 only goes to x/D = 4; even at this last measurement station trace of condensation artificially increases the magnitude of rms fluctuations. However, the trends seen in the unheated jets are similar to that of our earlier data from a different facility (PS 2002) where the problem with condensation was absent. Detailed radial surveys, similar to Figure 10 are available for all other operating conditions mentioned in Table I.

A closer look into the rms data along the lip line (Figures 9 and 10) shows an interesting difference between the unheated and heated jets. The peak density fluctuations, at the first measurement station, appear close to the lip line. This peak position however moves inward towards the centerline in unheated jet, while in the heated jet the peak location moves radialy outward. To further examine this difference, density profiles from a single axial station are plotted in Figure 11. The figure shows that while profiles from all heated conditions are nearly self-similar, the profile of the unheated jet is narrower, perhaps indicative of slower spreading. Now, radial spreading seen via density measurement is found to be different from that seen via axial velocity measurement. Figure 12 presents a comparison of the present density data with velocity data measured in the same facility by Bridges and Wernet (2003). Note that the time-averaged velocity profiles of Figure 12(a) are self-similar: they collapse on a single line when plotted without shift. The density shear layer, on the other hand, lies inside of the velocity shear layer in the unheated jet, but moves outside whenever heating is introduced. Intuitively, the trend makes sense: in the unheated jet core density is higher than the ambient; therefore the growth of the shear layer is accompanied by higher density fluctuations in the core side. An opposite situation arises in heated jets where the ambient density is higher than the core. The Crocco-Busemann equation (White 1973) also predicts similar differences between heated and unheated conditions. The root-mean-square fluctuations data of Figure 12(b) shows a separation between the peak locations of density fluctuations and velocity fluctuations. The velocity and density data are from two different experiments and therefore, a small difference in the radial positions of the probe volume is expected. The differences

seen in Figure 12, however, are far bigger than the positioning error.

Leaving aside the difference between the heated and unheated conditions, when *only* the heated jets are considered, Figure 11 shows that the there exist no or very small difference in the spreading. This was also confirmed from the measured centerline data (not presented). To identify the changes in spreading due to heating, one needs to survey jets with constant fluid dynamic Mach number M_j that correctly identifies the compressibility effect. The present experiment was conducted in constant acoustic Mach number M_a where M_j is shown to decrease continually (Table I and Figure 2a) with increased heating. Earlier experiments (Lau 1981, Lepicovsky et al. 1988) have shown that the spreading rate increases with heating. The current trend (heated conditions only) is perhaps due to a cancellation between a decrease in the spreading rate due to the lowering of Mj, and an increase in the spreading rate due to increasing plume temperature.

Density fluctuations spectra: The density fluctuation spectra measured from the heated TR = 2.7 jet are shown in Figure 13. The power spectral density values are normalized by $(\rho_j - \rho_a)^2$. The potential core region of the jet has very little fluctuations, and the spectrum at x/D=3 Figure 13(a) is indicative of the electronic noise floor. Along the centerline the spectral energy grows as the end of the potential core is approached (x/D ~ 5); beyond which the spectra appears self-similar. The spectral energy is expected to decay farther downstream of the last measurement station. The peripheral shear layer (Figure 13b) was highly turbulent even at the first measurement station: x/D = 0.25. In fact the spectral energy level is the highest in the first measurement station than all other downstream locations. The rms density fluctuations data, presented earlier, show that the peak fluctuation region moves radialy away from the lip line. This is the reason for the lowering of spectral energy seen in Figure 13(b). A comparison with earlier measurements (PS 2002) in unheated jets shows significant differences in the density spectra measured along the shear layer. The data of PS 2002 showed a progressive increase in the energy level with downstream distance. The spectral shape was also different: a hump at St ~ 4 was present in the spectrum close to the nozzle exit. The hump progressively moved to lower Strouhal frequencies with downstream distance. The behavior was typical of a quasi-laminar shear layer going through transition to full turbulence. The data of Figure 13(b) however indicates a fully turbulent shear layer right at the nozzle exit and the absence of any transition process. The state of the initial shear layer will soon be elaborated.

The spectra from plumes of different temperature ratios are compared in Figure 14. Notably, the spectra from heated conditions show little difference within measurement uncertainty. The unheated jet data in Figure 14(b) however stands out to show higher energy level. The difference might be due to the radial shifting of the density shear layer as described earlier. In addition spectra from the unheated jet have a higher noise floor due to trace condensation. Nevertheless, it is reasonable to conclude that the density fluctuations spectra remain nearly unaffected by changing plume temperature. This is in contrast to the far field noise spectra where heating is shown to significantly reduce the high frequency noise emission (St > 0.8) at all polar angles.

Initial shear layer: The status of the initial shear layer slightly downstream (x/D = 0.25) of the nozzle exit is investigated in Figures 15 and 16. The time averaged density profiles of Figure 15, at all plume temperatures, are nearly similar. The interesting feature is that the peak rms fluctuations in the lip shear layer increases with increased plume temperature. The density fluctuations spectra in Figure 16 provide additional support. The spectra show that the unheated jet has far lower energy levels at the lower frequencies than any of the heated jets. The spectra from the unheated jet shows a hump around St = 4, similar to the quasi-laminar shear layer of PS 2002. Noticeably, the low frequency part of the spectrum increases with increased plume temperature. It has been discussed earlier that heating at constant M_a reduces Reynolds number. Table I shows Reynolds number reduction from 1.4 Million in the unheated condition to 0.2 Million in TR = 2.7 jet. Therefore, before the test, the expectation was to find laminarization of the initial shear layer with increased heating. Figure 16 shows an opposite trend: an increase of the fluctuation level with heating. A plausible explanation lies with the deteriorating performance of the contraction section of the nozzle block with increased plume temperature. It is known that the wall boundary layer at the beginning of a contraction section experiences adverse pressure gradient due to curvature of streamlines (Morel 1975). Since the flow velocity is very low, small local separation is not uncommon. Such flow separations have been seen in some low speed wind tunnel contractions (Whitehead and Walters 1951). Once separated, turbulent fluctuations, rich in low frequency content, pass to the exit shear layer via wall boundary layer. In the present experiment the lowering of Reynolds number with heating perhaps has initiated such separation leading to the increased turbulence in the exit shear layer.

M_a = 0.9 flow-sound correlation: The correlation data between turbulent density fluctuations in the plume and the far-field sound pressure fluctuations are expressed in terms of coherence spectrum $\Gamma^2_{\rho',p'}(St)$ which is a measure of linear dependency between the two. A coherence value of unity implies a perfectly linear cause and effect relation while a value of zero implies no correlation. It has been pointed out earlier that the present coherence data are biased towards lower value due to contributions from electronic shot noise. Also, zero value of the coherence function was never realized, instead a noise floor around $\Gamma^2_{\rho',p'} \sim 0.01$ was reached. When the coherence level is above the noise floor, it can be said that some part of density fluctuations from the laser probe location is creating sound pressure fluctuations at the microphone location; in other words, the probe location is a sound source. Figure 17 shows typical polar angle dependence of the coherence function when the probe volume is placed at the strongest sound producing region. Coherence levels above the noise floor were found only in the low frequency St<0.8 range. Additionally, correlations are the highest in the shallowest polar angle. As the polar angle is decreased towards 90° the coherence value diminishes. The observations are consistent with earlier measurements of PS 2002 and Panda, Seasholtz and Elam (2003) where it has been argued that the correlation technique identifies contributions from large-scale turbulent fluctuations while that from the fine scale fluctuations go below experimental noise floor. Figure 18 shows that the strongest noise sources lies along the jet

centerline and downstream of the end of the potential core. The peripheral shear layer shows weaker correlation with the shallow angle noise and almost no correlation with the 90° microphone signal (not shown).

The correlation data from all other heated conditions at $M_a = 0.9$ (except for that shown in Figure 19) were similar to that of Figures 17 and 18, which indicate that the low frequency noise source remains unchanged with heating at least for this acoustic Mach number. This is consistent with the far field noise spectra of Figure 8(a). The far field noise spectra show significant difference in higher frequency; the present technique is unable to identify sources for this part of the spectrum.

Figure 19 presents an interesting scenario, when slight elevation of the plenum temperature produced a plume where static temperature is nearly the same as that of the ambient. Therefore, the core density is the same as that of the ambient. Although, the radial density profiles obtained from this jet (not shown) show slight lowering at the center of the shear layer due to viscous heating. Figure 19 demonstrates that the correlation values are far lower than those in either heated or unheated conditions. Note that the far field noise emission, at least the low frequency part, remains unchanged between unheated, temperature balanced and unheated jets. This provides insight into the interpretation of correlation data. The density fluctuations have basically acted as a 'tracer' for the noise sources. In the temperature balanced jet the 'tracer' becomes weak, leading to the weakening of the correlation values. Therefore, it is impossible to separate noise sources from density fluctuations alone, and for that matter any other variables: temperature, velocity, entropy etc. The sound source description in any variable is related to all others.

TR = 2.27 plume survey: In the following data obtained from a fixed temperature ratio of 2.27 but at 3 different $M_a = 0.6$, 0.9, and 1.48 are presented. The far field noise spectra measured by Tanna et al (1976) for these operating conditions are shown in the Appendix A. Figure 20 provides a comparison of the centerline decay for the 3 jets. An increase in M_a is accompanied by a similar increase in the jet Mach number and the associated lowering of the shear layer growth rate. This manifests in a longer potential core length with increasing M_a. The density fluctuations spectra in Figure 21 shows near similarity, except for the differences in the low frequency end, at all Mach number conditions. PS 2002 has found similar results over a wider Mach number range in unheated jets via detailed survey over the entire plume. Except for a lowering of the growth rates, the single point statistics of turbulence fluctuations fundamentally remain similar over the subsonic and low supersonic range considered in these experiments.

TR = 2.27 flow-sound correlation: Finally Figures 22 and 23 provide a comparison of the correlations measured in $M_a = 0.6$ and 1.48 jets. The two parts in each figure show data from the peripheral shear layers and the centerlines of the jets. In general, correlations from the supersonic (relative to the ambient sound speed) plume are higher in magnitude and appear over a larger Strouhal frequency range than those measured from the subsonic plume. The differences are most significant along the peripheral shear layer where the strong correlations found in the $M_a = 1.48$ jet are mostly absent in the $M_a = 0.6$ jet. Similar results from unheated jets were presented by PS 2002 and Panda, Seasholtz and Elam 2003. The differences were attributed to the presence or absence of Mach wave radiation process from the Kelvin-Helmholtz instability waves. The convective velocity of the instability waves in the $M_a = 0.6$ jet is lower than that of the ambient sound speed, while instability waves in the $M_a = 1.48$ jet are expected to attain speed higher than the ambient. Therefore, the plume and near field fluctuations in the latter are strongly correlated with the far field radiation. The air density fluctuations from the centerline and downstream of the potential core are always found to be a strong sound source at all M_a and temperature ratios as demonstrated from the earlier as well as the present data.

SUMMARY AND CONCLUSION:

A molecular Rayleigh scattering based density measurement technique was used in the Small Hot Jet Acoustic Rig of the Aero-Acoustic Propulsion Laboratory ("Dome") to investigate turbulence properties and noise sources of hot, high speed jets. Rayleigh scattering has been used in the past to diagnose noise sources in unheated jets (Panda and Seasholtz 2002); this was the first test in heated jets. The goals were threefold: to determine whether a Rayleigh diagnostic is feasible in the rugged environment of the Dome, to further add to a flow and acoustic database and to characterize the changes caused by heating. The database being created by multiple researchers, and is intended to aid various computational code developments.

The facility was cleansed of dust particles from the past PIV tests, and a clean low speed co-flow system was added to avoid large scattering from particles. A hydrogen combustor was used to heat the jet and to avoid soot particles. These precautions helped to demonstrate viability of a Rayleigh scattering technique in the facility. A large amount of flow and acoustic data was obtained over different acoustic Mach numbers and temperature ratios. Additionally, unsteady density fluctuations in the jet and far field sound pressure fluctuations were measured simultaneously. A cross-correlation between the two fluctuations provided the low frequency noise sources in the jet.

This paper presents data from two sets of operating conditions. For the first set M_a was kept fixed at 0.9 and temperature ratio was varied between 0.84 (unheated) and 2.7. This set of data shows the effect of elevating plume temperature on flow turbulence and far field noise. For the second set the temperature ratio was kept fixed at 2.27 and the M_a was varied between 0.6 and 1.48. This set demonstrates the effect of the changing velocity.

Detailed surveys of the time-averaged density and density fluctuation spectra were conducted in all plumes. The time averaged density measurements in the first set of data showed differences in the peripheral density shear layers between the unheated and heated jets. While radial profiles from all heated jet are nearly similar, those of the unheated jet lie closer to the jet axis. Comparisons with earlier axial velocity data from PIV survey of Bridges and Wernet (2003) show that in the unheated jet, the density shear layer hugs the inside edge of the velocity shear layer. In heated jet the density shear layer lies on the outside edge. Radial profiles measured in the *heated conditions* showed very small increase in spreading. On the other hand,

surveys made in the second set show significant changes in the spreading associated with increased jet Mach number.

The density fluctuations spectra measured at the closest axial station, x/D = 0.25 and at the middle of the lip shear layer showed unexpected increase in the low frequency content with increased heating. It is conjectured that the lowering of Reynolds number deteriorated the performance of the nozzle block; local separation at the beginning of the contraction section might have caused increased turbulence in the initial shear layer. The downstream development of the lip shear layer was typical of a fully turbulent one, unlike the transitional behavior seen in unheated jets of Panda and Seasholtz (2002). Further downstream from the nozzle exit the density fluctuations spectra normalized by $(\rho_j-\rho_a)^2$ were similar for all temperature ratio and Mach number conditions (except for the change associated with stretching with increased M_a). This demonstrated a near universality of single point statistics of the turbulence field.

The far field noise spectra, however, was vastly different for different operating conditions. Spectra measured by Tanna, Dean and Burrin (1976) were plotted to recount the differences at various M_a and TR. For the $M_a = 0.9$ jets noise spectra from the shallow radiation angle showed that the low frequency part ($St < 0.8$) remains unaffected by heating while the high frequency part continually decreases. The high frequency part at shallow angle, however, is found to scale with $\rho_j U_j^2$.

Similar to the previous measurements of Panda and Seasholtz (2002) and Panda, Elam and Seasholtz (2003), the correlation measurements between turbulent density fluctuations and far field sound pressure fluctuations showed the region beyond the end of potential core to be the strongest noise source for low frequency emission ($St < 0.5$). The inception of the Mach wave radiation process in the $M_a = 1.48$ jet made the peripheral shear layer also a significant noise source. This was unlike $M_a < 1$ jets, where weaker correlations were measured from the shear layer. Increasing the plume temperature did not change the scenario, except for the interesting case of an isothermal jet where plume and ambient density were nearly equal. The small turbulent density fluctuations were found to be poorly correlated with the far field noise. This showed that the density fluctuations behaved as a 'tracer variable' to the noise sources. The additional implication is that, at least for the low frequency sources, it is impossible to isolate contributions from individual variables such as velocity, density or temperature.

References

Bridges, J. and Wernet, M.P., "Measurements of the Aero-acoustic Sound Source in Hot Jets" AIAA-2003- 3130, 9th AIAA/CEAS Aeroacoustics Conference, Hilton Head, South Carolina, May 12-14, 2003.

Castner, R.S., 1994, "The Nozzle Acoustic Test Rig: An Acoustic and Aerodynamic Free-Jet Facility," *NASA TM 106495*.

Crighton, D.G. 1975 Basic principles of aerodynamic noise generation, *Prog. Aerospace Sci.*, **16**(1), 31-96.

Fisher, M.J., Lush, P.A., and Harper Bourne, M. 1973 Jet noise *J. Sound & Vib.*, **28**(3), 563-585.

Fortuné, V. and Gervais, Y. 1999 Numerical investigation of the noise radiated from hot subsonic turbulent jets, *AIAA J.* **37**(9), pp 1055-1061.

Kerhervé, F., Jordan, P., Gervais, Y., and Valiere, J.C. 2003 Aerodynamic characterization of a supersonic jet using two-point laser Doppler Velocimetry, *AIAA paper2003-3215*.

Lau, J.C. 1981 Effects of exit Mach number and temperature on mean flow and turbulence characteristics in round jets, *J. Fluid Mech.*, **105**, pp 193-218.

Lepicovsky, J., Ahuja, K.K., Brown, W.H., Salikuddin, M., and Morris, P.J. 1988 Acoustically excited heated jets, Part III—mean flow data, *NASA CR 4129*.

Lighthill, M.J. 1954 On sound generated aerodynamically I. General theory. *Proc. Royal Soc.*, **A221** 564-587.

Lourenco, L.M. and Krothapalli, A. 1995 On the Accuracy of Velocity and Vorticity Measurements with PIV, *Experiments in Fluids* **18**, 421-428.

Miles, R. B., Lempert, W. R. and Forkey, J. N. 2001 Laser light scattering, *Meas. Sci Technol.,* **12**, R33- R51.

Mollo-Christensen, E. and Narasimha, R. 1960 Sound emission from jets at high subsonic velocities, *J. Fluid Mech.,* **8**, 49-60.

Morel, T. 1975 Comprehensive design of axisymmetric wind tunnel contractions, *ASME paper 75 FE-17.*

Whitehead, L.G., Wu, L.Y., and Waters, M.H.L. 1951 Contracting ducts of finite length, *The Aeronautical Quarterly*, Vol. **II,** 254-271.

Panda, J. and Seasholtz, R.G. 2002 Experimental investigation of density fluctuations in high speed jets and correlation with generated noise. *J. Fluid Mech.* **450**, pp 97-130.

Panda, J., Seasholtz, R.G., and Elam, K.A. "Further Progress in Noise Source Identification in High Speed Jets Via Causality Principle", AIAA paper 2003-3126, also submitted to *Journal of Fluid-Mechanics*.

Panda, J., Seasholtz, R.G., Elam, K.A., and Mielke, A.F. 2004 Time-averaged velocity, temperature and density surveys of supersonic free jets, *ASME paper number HT-FED2004-56856*.

Pitts, W.M., and Kashiwagi, T. 1984 The application of laser-induced Rayleigh scattering to the study of turbulence mixing. *J. Fluid Mech.*, **141** 391-429.

Schaffer, M. 1979 Direct measurements of the correlation between axial in-jet velocity fluctuations and far field noise near the axis of a cold jet. *J. Sound & Vib.* **64**(1) 73-83.

Seiner, J.M. and Reethof, G. 1974 On the distribution of source coherency in subsonic jets. *AIAA paper 74-4*

Siddon, T.E. 1973 Noise source diagnostics using causality correlations, *AGARD CP 131, Noise Mechanisms* 7-1:7-13.

Tam, C.K. W. 2001 On the failure of the Acoustics Analogy Theory to identify the correct noise sources. *AIAA paper no 2001-2117.*

Tam, C.K.W. and Ganesan, A. 2004 Modified k-ε turbulence model for calculating hot jet mean flows and noise, *AIAA J.* **42**(1) pp 26-34.

Tanna, H.K. 1977 An experimental study of jet noise, Part I: Turbulent mixing noise, *JSV,* **50**(3), pp 405-428

Tanna H.K., Dean P.T., and Burrin R.H. 1976 The generation and radiation of supersonic jet noise, Vol. III Turbulent Mixing Noise data, *Air Force Aero-Propulsion Laboratory Report AFAPL-TR-65*.

Viswanathan, K. 2001 Quality of jet noise data: issues, implications and needs, *AIAA paper 2001-2115*.

Welch, P.D. 1967 The use of fast Fourier transform for the estimation of power spectra: A method based on time averaging over short, modified periodograms, *IEEE Trans. on Audio and Electroacoustics,* **AU-15** 70-73.

White, F.M. 1973 *Viscous Fluid Flow*, McGraw-Hill, New York.

Table I: Operating conditions

M_a $=U_j/a_o$	TR $=T_j/T_a$	T_{plen} (K)	M_j $=U_j/a_j$	Uj	ρ_j/ρ_a	Re $_{X10^6}$	γ	Tanna point
0.90	0.840	289	0.982	306	1.19	1.41	1.3999	7
0.90	1.000	335	0.900	306	1.00	1.03	1.3995	12
0.90	1.429	458	0.754	306	0.70	0.55	1.3947	19
0.90	1.818	569	0.671	306	0.55	0.37	1.3845	27
0.90	2.273	699	0.604	306	0.44	0.25	1.3690	36
0.90	2.700	821	0.557	306	0.37	0.19	1.3550	46*
0.60	2.273	675	0.402	204	0.44	0.17	1.3690	33
1.48	2.273	772	0.993	504	0.44	0.42	1.3690	39
1.48	2.700	893	0.916	504	0.37	0.32	1.3550	49*

* Higher temperature ratio (2.86) used by Tanna, Dean and Burrin (1976)

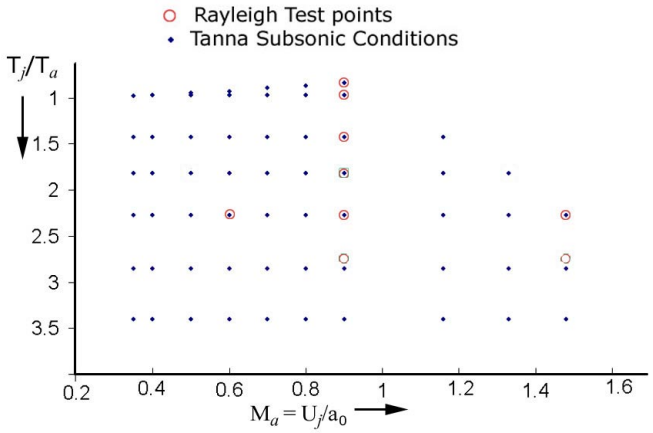

Fig. 1 Jet operating conditions. The blue dots are conditions used by Tanna, Dean and Burrin (1976) for a shock-free convergent nozzle and the red circles for the current experiment.

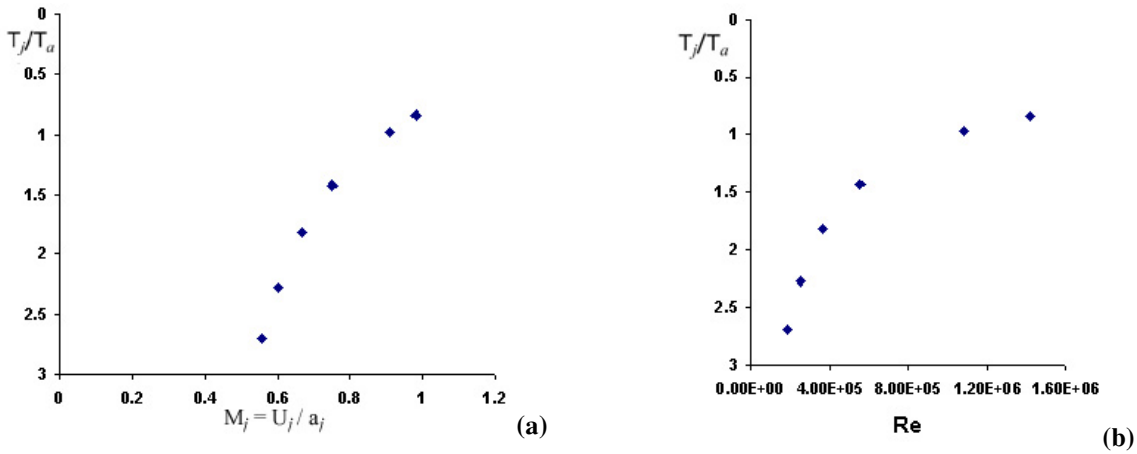

Fig. 2 (a) Jet Mach number M_j and (b) Reynolds number variations for test points representing constant acoustic Mach number $M_a = 0.9$.

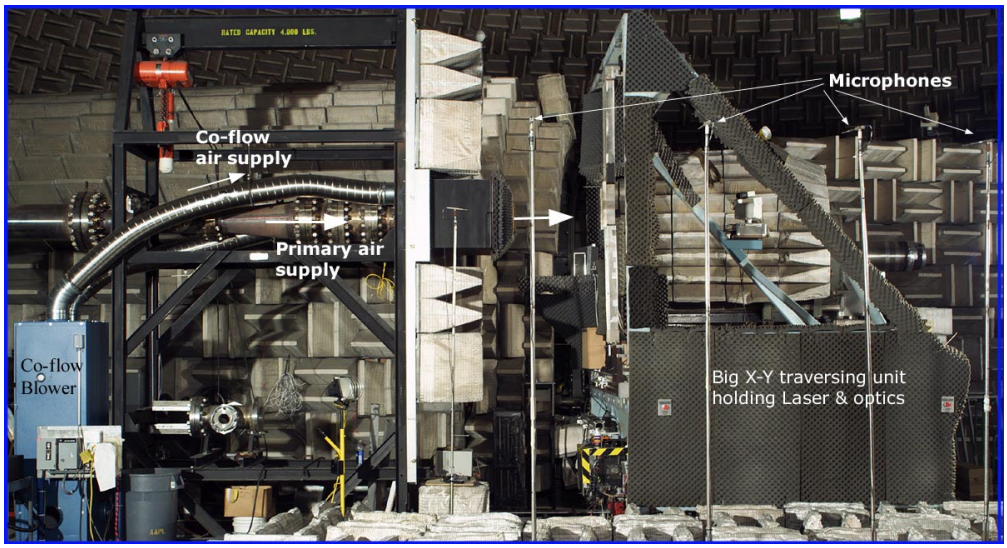

Fig. 3 Photograph showing side view of the Small Hot Jet Acoustic Rig, X-Y traverse holding the Rayleigh setup, and microphones.

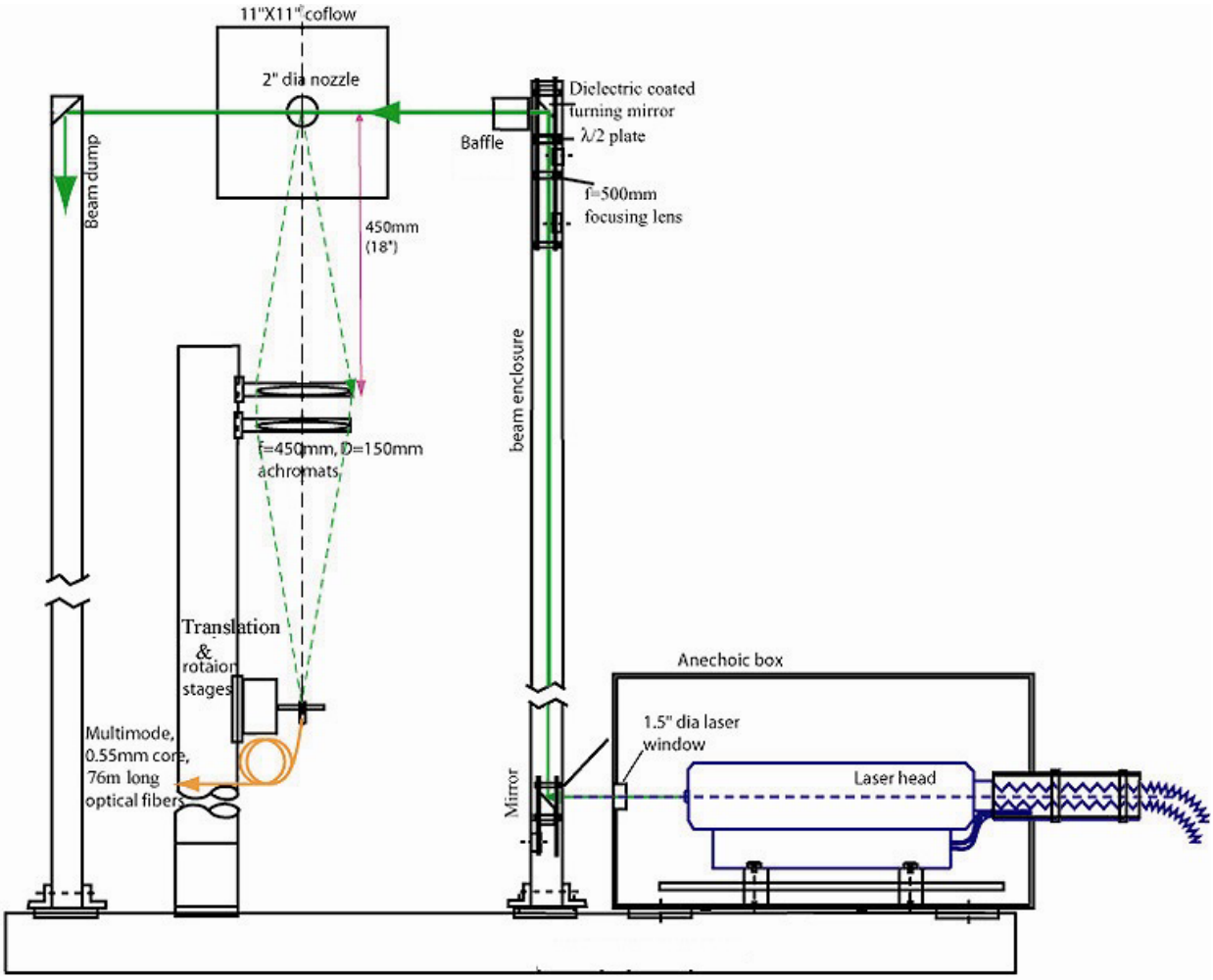

Fig. 4 A schematic of the part of Rayleigh setup around the jet facility

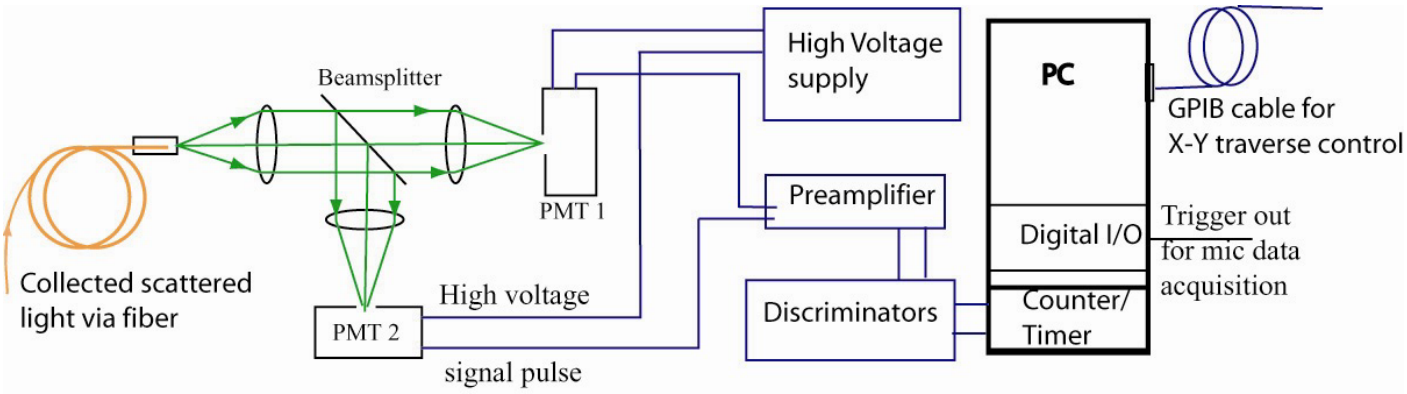

Fig. 5 A schematic of the optics and electronics used to measure scattered light intensity.

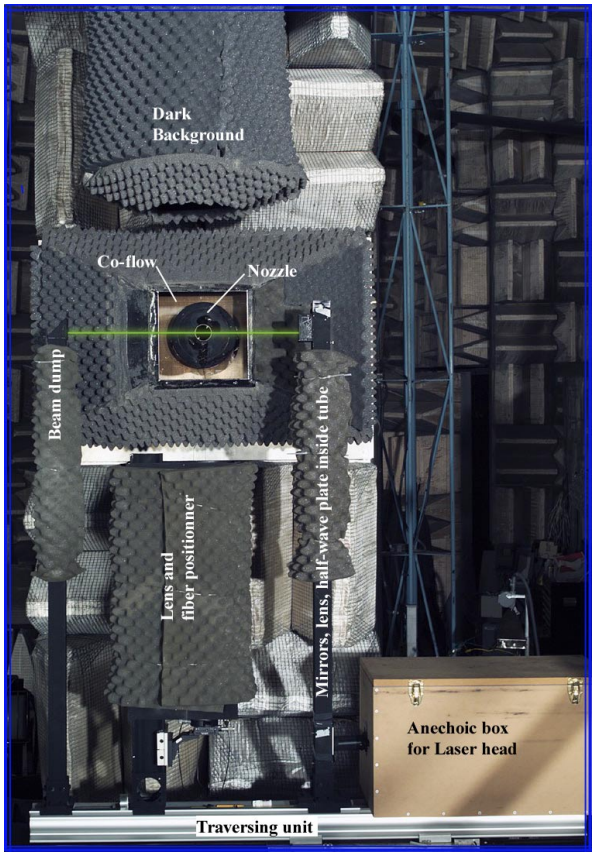

Fig. 6 Photograph showing the front view of the jet facility and the Rayleigh setup

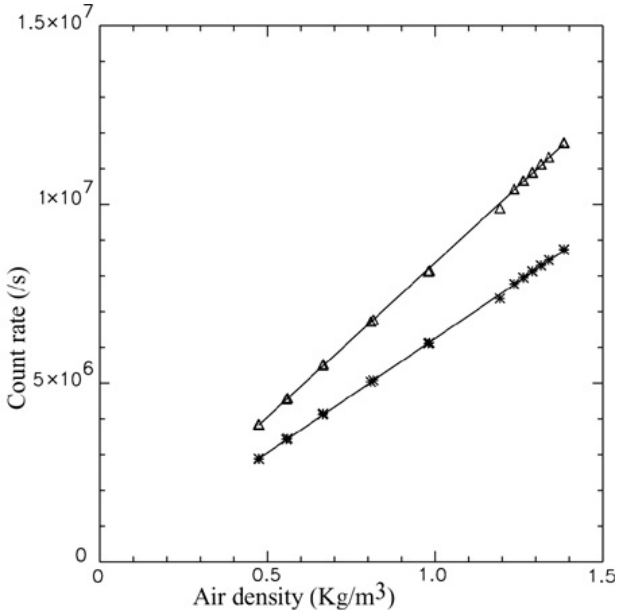

Fig. 7 Density calibration curves from 2 PMTs.

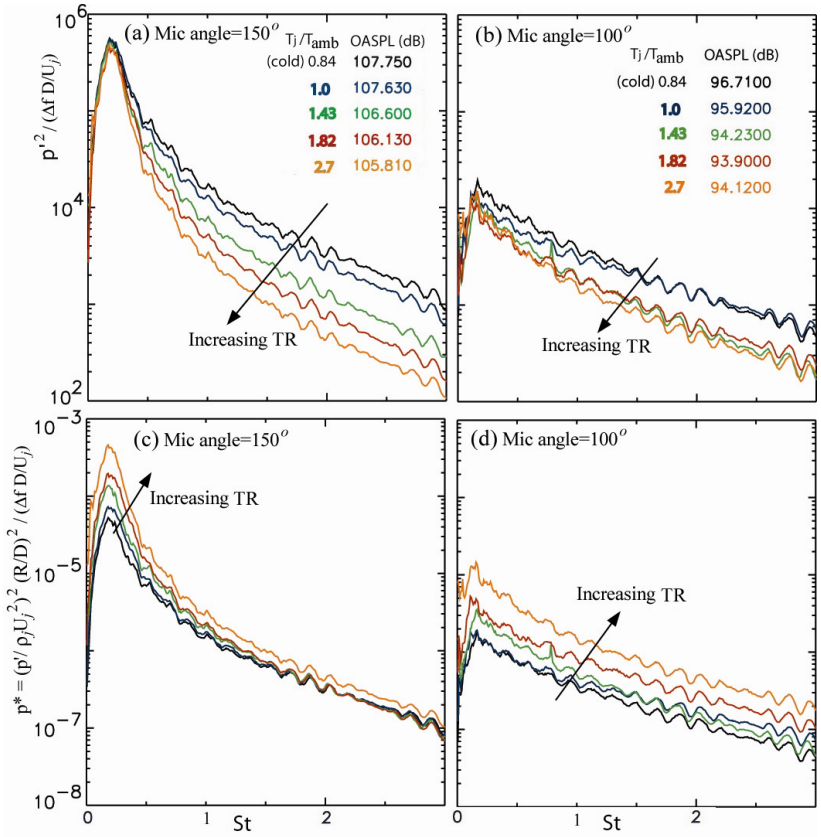

Fig. 8 Far field, narrowband, microphone spectra from indicated polar angles obtained from fixed $M_a = 0.9$ jets at indicated temperature ratios. (c) and (d) show the same data in (a) and (b) but normalized by a different factor.

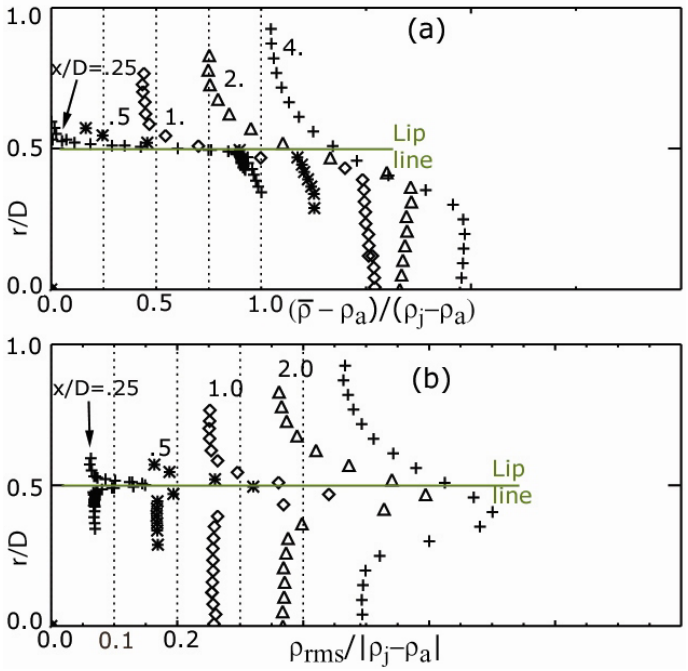

Fig. 9 Radial profiles of (a) mean and (b) rms density variations in unheated (TR = 0.84) M_a = 0.9 jet from indicated axial stations.

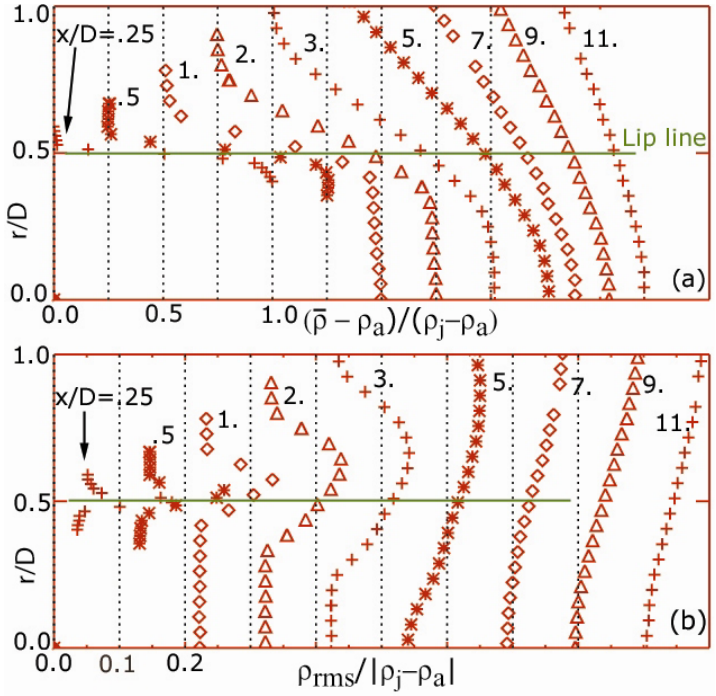

Fig. 10 Same as in Figure 9, but for a heated TR = 2.7 jet.

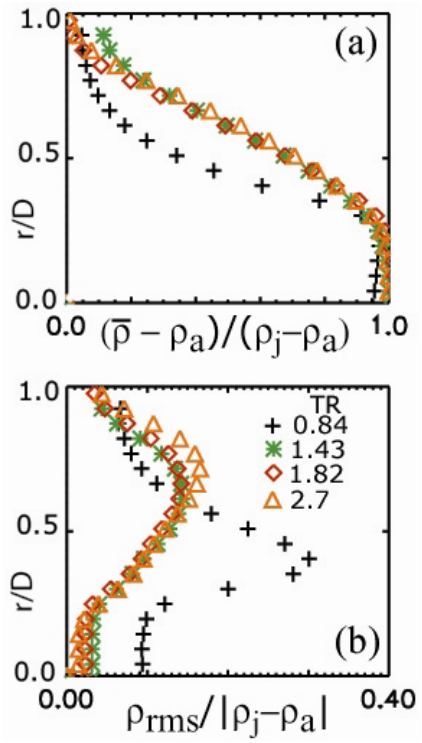

Fig. 11 Radial profiles of (a) mean and (b) rms density variation at fixed axial position of x/D=3, and fixed M_a = 0.9, but for different plume temperatures.

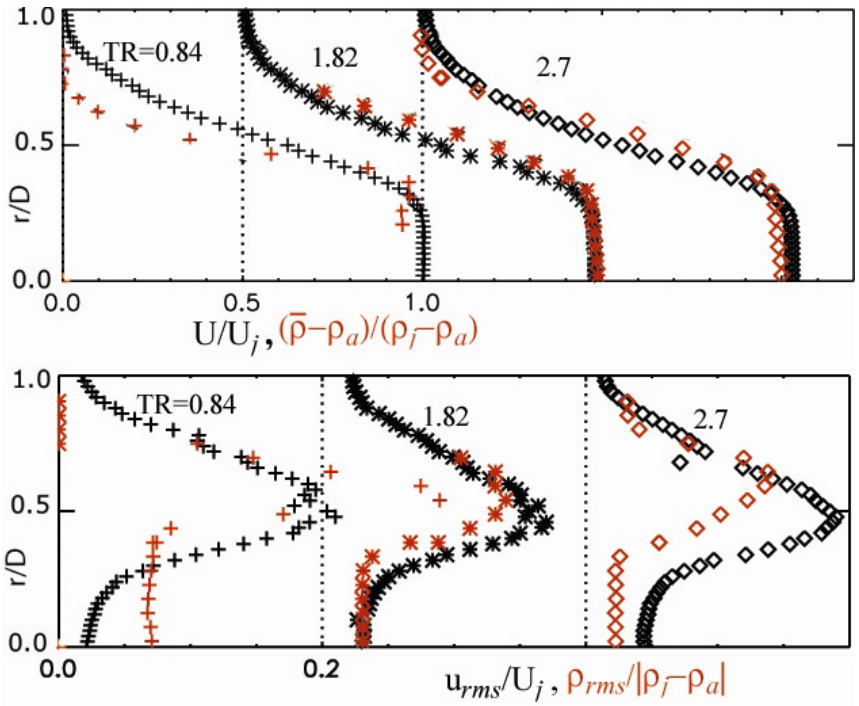

Fig. 12 Radial profiles of (a) mean axial velocity and density variations, (b) rms velocity and density variations from fixed axial position of x/D=3, and fixed M_a = 0.9, but for different plume temperatures. The axial velocity data were from PIV measurements of Bridges and Wernet (2003). The profiles are shifted by amounts shown by chain lines.

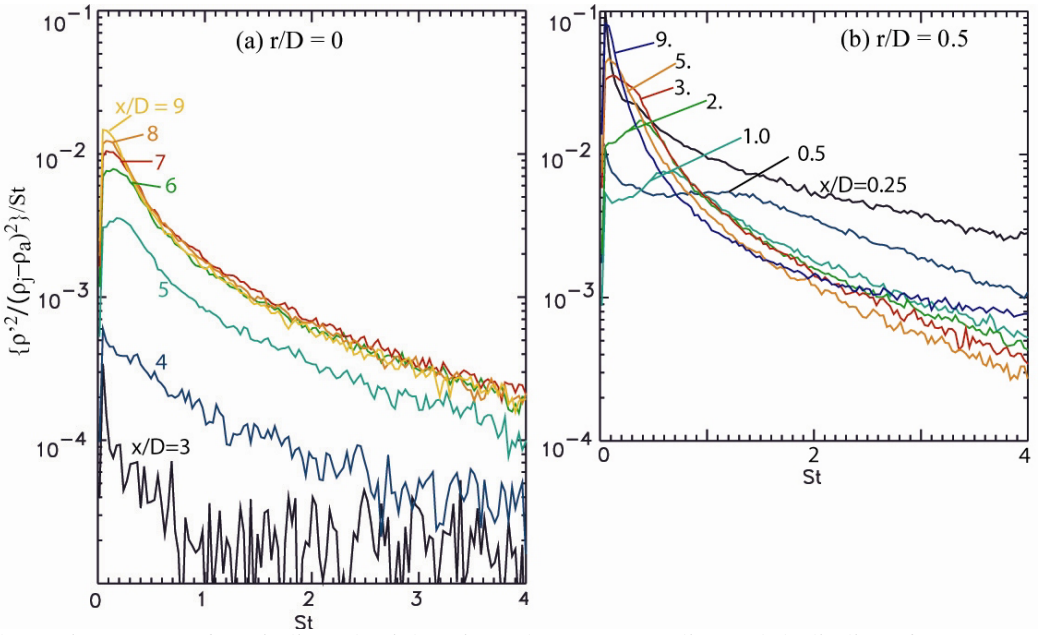

Fig. 13 Density fluctuations spectra from indicated axial stations along (a) centerline and (b) lip line of M_a = 0.9 and TR = 2.7 jet.

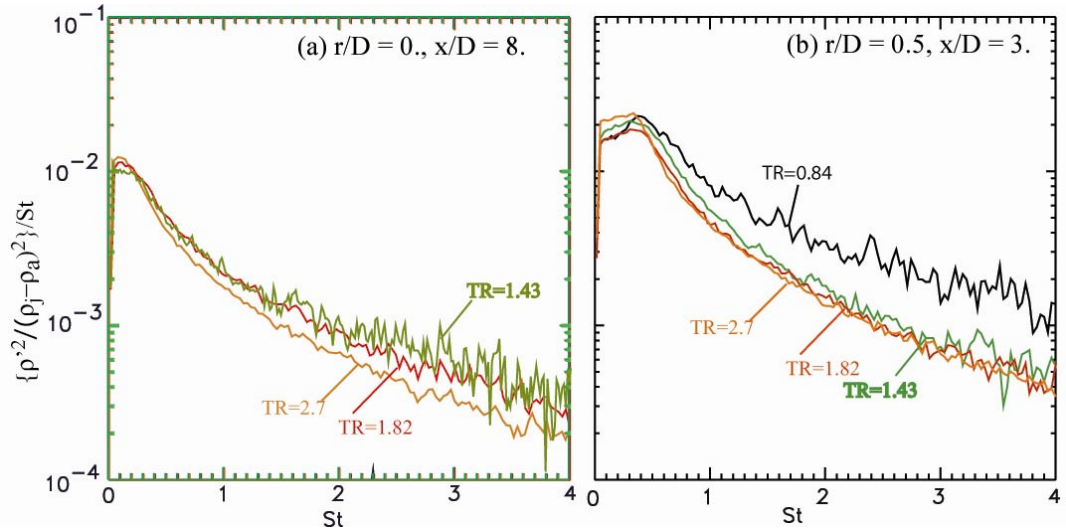

Fig. 14 Density fluctuations spectra from jets of different temperature ratios but fixed M_a = 0.9. Position of probe volume was kept fixed at (a) centerline and x/D = 8, (b) r/D=0.55 and x/D = 3.

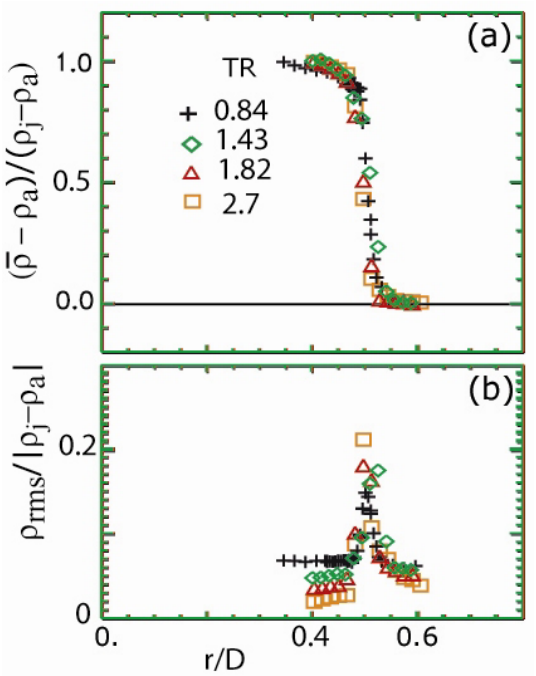

Fig. 15 Radial profiles of (a) mean and (b) rms density variation from close to the nozzle exit, x/D=0.25, from jets of different temperature ratios but fixed M_a = 0.9.

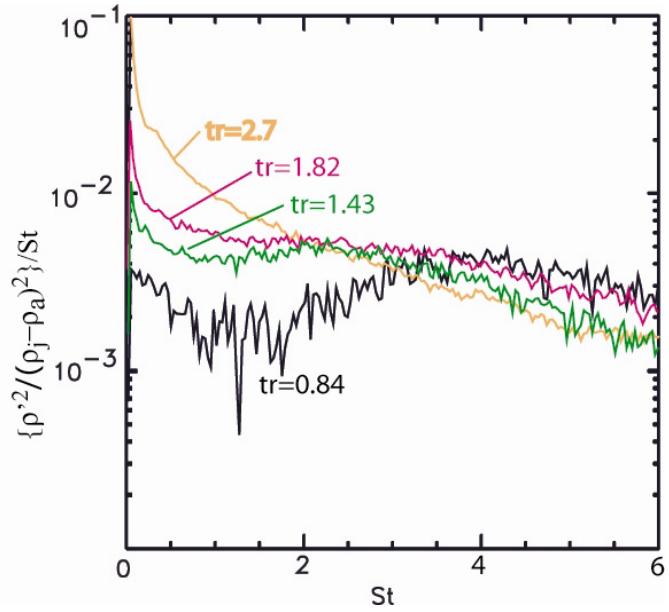

Fig. 16 Density fluctuations spectra from locations of maximum ρ_{rms} in lip shear layer close to the nozzle exit, x/D = 0.25. Data from jets of different temperature ratios but fixed M_a = 0.9.

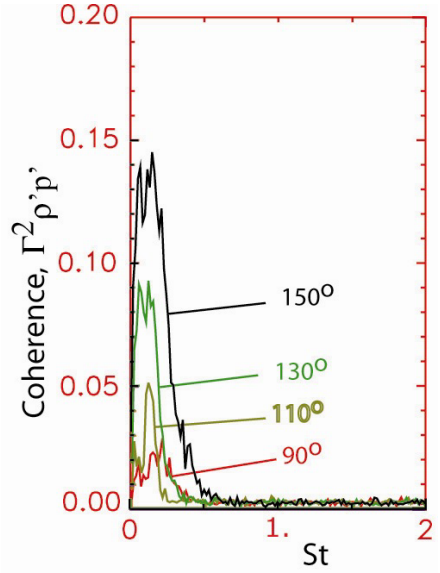

Fig. 17 Coherence spectra between air density fluctuations and far field sound pressure fluctuations measured at indicated microphone angular locations. Probe volume was fixed at centerline and x/D = 7 in M_a = 0.9 and TR = 2.7 jet. All microphones were 100D away from nozzle exit.

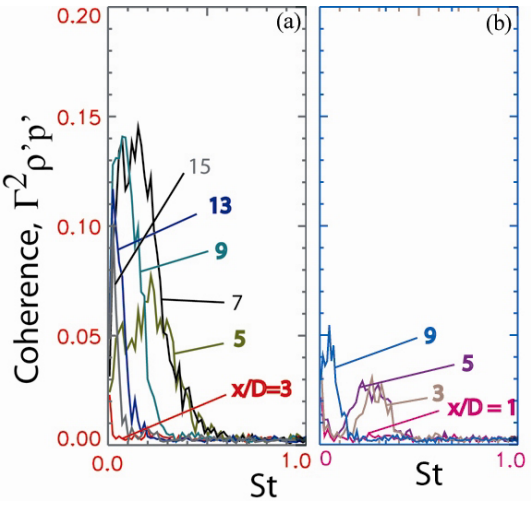

Fig. 18 Coherence spectra from a fixed microphone location of θ = 150° and R=100D but different probe volume location in M_a = 0.9 and TR = 2.7 jet. For (a) probe volume was kept at centerline but indicated axial position and for (b) probe volume at r/D=0.5 and indicated axial positions.

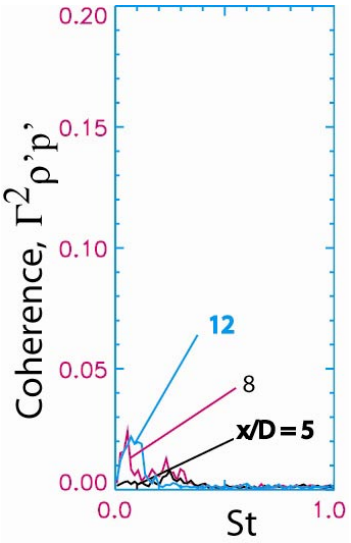

Fig. 19 Same as Figure 18(a) except TR = 1.0.

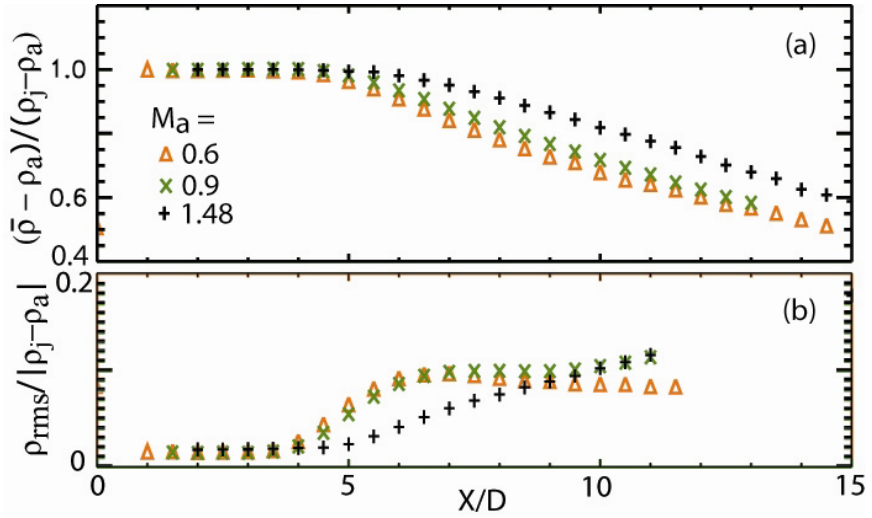

Fig. 20 Centerline variation of (a) time averaged density and (b) root-mean-square density fluctuations in jets with different indicated Mach numbers but fixed temperature ratio, TR = 2.27.

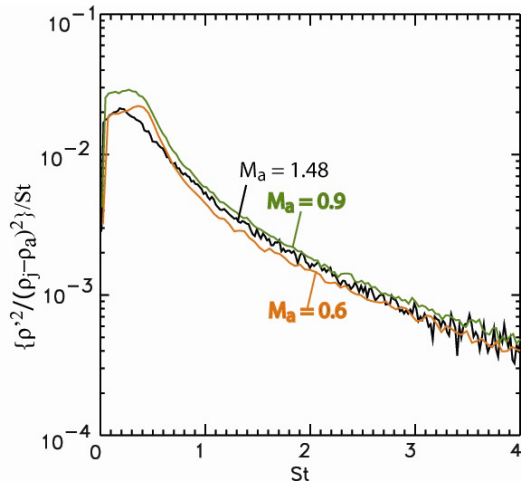

Fig. 21 Density fluctuations spectra from jets of different indicated Mach numbers but temperature ratio of TR=2.27. Probe volume was kept fixed at r/D=0.55 and x/D = 3.

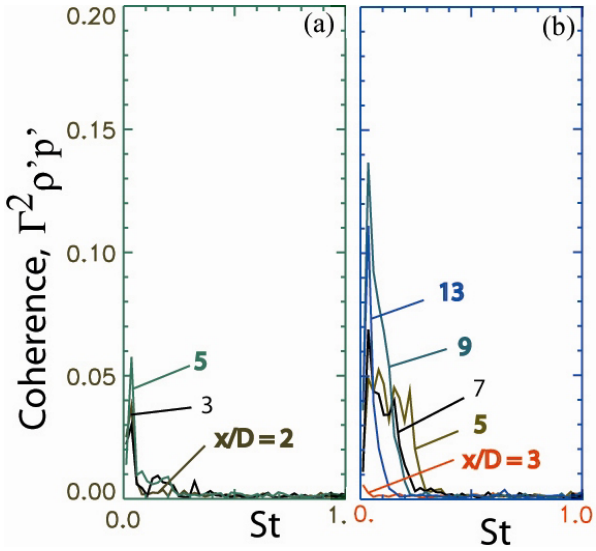

Fig. 22 Coherence spectra from a fixed microphone location of θ = 150° and R=100D but different probe volume location in M_a = 0.6 and TR = 2.27 jet. For (a) probe volume was kept at centerline but indicated axial position and for (b) probe volume was at r/D=0.5 and indicated axial positions.

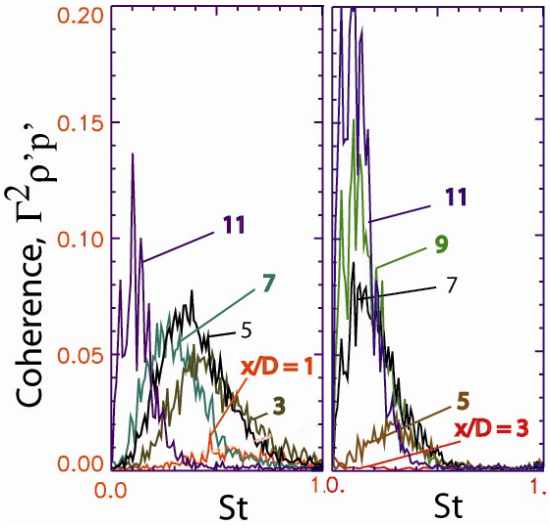

Fig. 23 Same as Figure 22, except M_a = 1.48.

APPENDIX A: Far field noise spectra measured by Tanna, Dean and Burrin (1976)

The operating conditions used in the present experiment are a subset of conditions used by Tanna, Dean and Burrin (1976). The emphases in the present work are on flow turbulence and sound source identification. The presence of a large traversing unit and optical components did not allow for clean noise spectrum measurements. Tanna et al, however, did not have this difficulty. Some of the tabulated spectra presented in their report are plotted in the Figure A1, which brings out the essential changes caused by heating. The figure shows that the spectral changes can be broadly classified based on Strouhal frequency. The high frequency side of the spectrum St > 0.8 is always reduced by heating at a fixed jet velocity. This is true even for the forward arc. Since, reduction beyond the cone of silence can not be attributed to refraction; the noise sources responsible for the high Strouhal frequency emission are weakened. The behavior of the lower frequency part, St < 0.8, is definitely Mach number dependent. For M_a=0.9 (middle column) the low frequency side is unaffected by heating. Yet if the acoustic Mach number is lowered, the low frequency sound levels increase with heating; and if Mach number is increased the sound level decreases with heating. This discussion does not account for the lowering of the thrust due to lower plume density caused by heating.

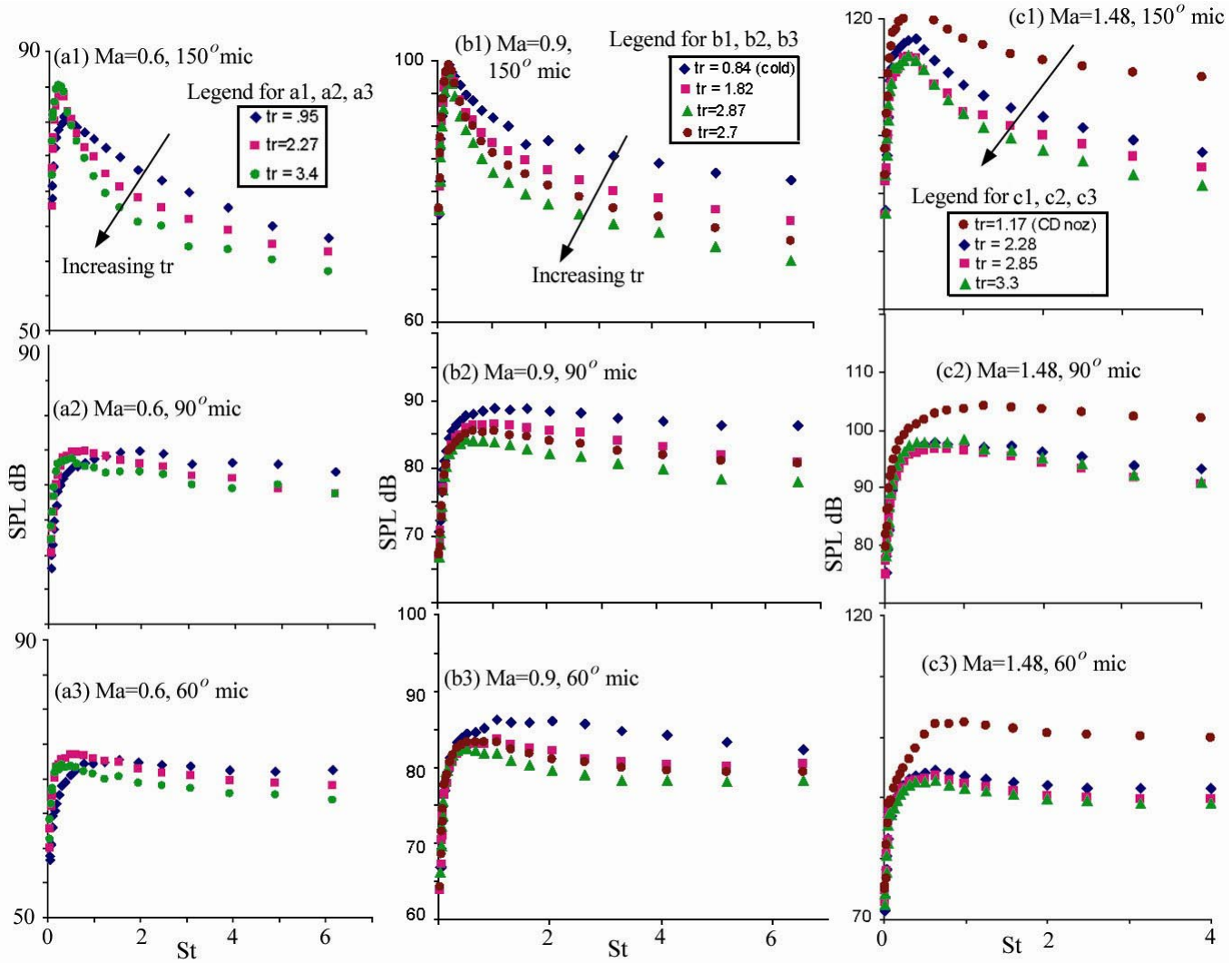

Fig. A1 Far field noise spectra from jets produced by 50.8 mm diameter nozzle at different M_a and TR. Columns (a), (b), and (c) presents data at M_a = 0.6, 0.9, and 1.48 respectively; rows (1), (2), and (3) are from different microphone angles θ = 150°, 90°, and 60° respectively. All microphones were positioned on a 72 diameters arc. All data are from a convergent nozzle except for a convergent-divergent nozzle for the unheated M_a = 1.48 jet.

REPORT DOCUMENTATION PAGE

Form Approved
OMB No. 0704-0188

1. AGENCY USE ONLY (*Leave blank*)	2. REPORT DATE	3. REPORT TYPE AND DATES COVERED
	June 2004	Technical Memorandum

4. TITLE AND SUBTITLE

Effect of Heating on Turbulent Density Fluctuations and Noise Generation From High Speed Jets

5. FUNDING NUMBERS

WBS–22–714–09–24

6. AUTHOR(S)

Jayanta Panda, Richard G. Seasholtz, Kristie A. Elam, Amy F. Mielke, and Dennis G. Eck

7. PERFORMING ORGANIZATION NAME(S) AND ADDRESS(ES)

National Aeronautics and Space Administration
John H. Glenn Research Center at Lewis Field
Cleveland, Ohio 44135–3191

8. PERFORMING ORGANIZATION REPORT NUMBER

E–14620

9. SPONSORING/MONITORING AGENCY NAME(S) AND ADDRESS(ES)

National Aeronautics and Space Administration
Washington, DC 20546–0001

10. SPONSORING/MONITORING AGENCY REPORT NUMBER

NASA TM—2004-213126
AIAA–2004–3016

11. SUPPLEMENTARY NOTES

Prepared for the Tenth Aeroacoustics Conference cosponsored by the American Institute of Aeronautics and Astronautics and the Confederation of European Aerospace Societies, Manchester, United Kingdom, May 10–12, 2004. Jayanta Panda, Ohio Aerospace Institute, Brook Park, Ohio 44142; Richard G. Seasholtz and Amy F. Mielke, NASA Glenn Research Center; Kristie A. Elam, Akima Corporation, Fairview Park, Ohio 44126; and Dennis G. Eck, QSS Group, Inc., Cleveland, Ohio 44135. Responsible person, Jayanta Panda, organization code 5940, 216–433–8891.

12a. DISTRIBUTION/AVAILABILITY STATEMENT

Unclassified - Unlimited
Subject Category: 45 Distribution: Nonstandard

Available electronically at http://gltrs.grc.nasa.gov

This publication is available from the NASA Center for AeroSpace Information, 301–621–0390.

12b. DISTRIBUTION CODE

13. ABSTRACT ***(Maximum 200 words)***

Heated jets in a wide range of temperature ratios (TR), and acoustic Mach numbers (M_a) were investigated experimentally using far field microphones and a molecular Rayleigh scattering technique. The latter provided density fluctuations measurements. Two sets of operating conditions were considered: (1) TR was varied between 0.84 and 2.7 while M_a was fixed at 0.9; (2) M_a was varied between 0.6 and 1.48, while TR was fixed at 2.27. The implementation of the molecular Rayleigh scattering technique required dust removal and usage of a hydrogen combustor to avoid soot particles. Time averaged density measurements in the first set of data showed differences in the peripheral density shear layers between the unheated and heated jets. The nozzle exit shear layer showed increased turbulence level with increased plume temperature. Nevertheless, further downstream the density fluctuations spectra are found to be nearly identical for all Mach number and temperature ratio conditions. To determine noise sources a correlation study between plume density fluctuations and far field sound pressure fluctuations was conducted. For all jets the core region beyond the end of the potential flow was found to be the strongest noise source. Except for an isothermal jet, the correlations did not differ significantly with increasing temperature ratio. The isothermal jet created little density fluctuations. Although the far field noise from this jet did not show any exceptional trend, the flow-sound correlations were very low. This indicated that the density fluctuations only acted as a "tracer parameter" for the noise sources.

14. SUBJECT TERMS	15. NUMBER OF PAGES
Rayleigh scattering; Jet aircraft noise	23
	16. PRICE CODE

17. SECURITY CLASSIFICATION OF REPORT	18. SECURITY CLASSIFICATION OF THIS PAGE	19. SECURITY CLASSIFICATION OF ABSTRACT	20. LIMITATION OF ABSTRACT
Unclassified	Unclassified	Unclassified	